arXiv:1606.04438v2 [physics.flu-dyn] 20 Jun 2016

Distributed chaos in turbulent wakes

A. Bershadskii
ICAR, P.O. Box 31155, Jerusalem 91000, Israel

Soft and hard spontaneous breaking of space translational symmetry (homogeneity) have been studied in turbulent wakes by means of distributed chaos. In the case of the soft translational symmetry breaking the vorticity correlation integral $\int_V \langle \boldsymbol{\omega}(\mathbf{x},t)\cdot\boldsymbol{\omega}(\mathbf{x}+\mathbf{r},t)\rangle_V d\mathbf{r}$ dominates the distributed chaos and the chaotic spectra $\exp -(k/k_\beta)^\beta$ have $\beta = 1/2$. In the case of the hard translational symmetry breaking, control on the distributed chaos is switched from one type of fundamental symmetry to another (in this case to Lagrangian relabeling symmetry). Due to the Noether's theorem the relabeling symmetry results in the inviscid helicity conservation and helicity correlation integral $I = \int \langle h(\mathbf{x},t)\, h(\mathbf{x}+\mathbf{r},t)\rangle d\mathbf{r}$ (Levich-Tsinober invariant) dominates the distributed chaos with $\beta = 1/3$. Good agreement with the experimental data has been established for turbulent wakes behind a cylinder, behind grids (for normal and super-fluids) and for bubbling flows. In the last case even small concentration of bubbles leads to a drastic change of the turbulent velocity spectra due to the hard spontaneous symmetry breaking in the bubbles' wakes.

SOFT AND HARD SPONTANEOUS SYMMETRY BREAKING

The spontaneous breaking of space translational symmetry (homogeneity) has been studied for the first time for *weak* turbulence in a recent paper Ref. [1]. For *strong* turbulence it was studied in Ref. [2] by means of the distributed chaos. It was shown in the Ref. [2] that in one of the possible scenarios scaling of the group velocity of the waves (pulses) driving the distributed chaos

$$v(\kappa) \propto |\gamma|^{1/2}\ \kappa^{\alpha} \tag{1}$$

is dominated by the vorticity correlation integral

$$\gamma = \int_V \langle \boldsymbol{\omega}(\mathbf{x},t)\cdot\boldsymbol{\omega}(\mathbf{x}+\mathbf{r},t)\rangle_V d\mathbf{r} \tag{2}$$

with $\alpha = 1/2$ from the dimensional considerations. It results in the chaotic stretched exponential spectra

$$E(k) \propto \exp -(k/k_\beta)^\beta \tag{3}$$

with

$$\beta = \frac{2\alpha}{1+2\alpha} \tag{4}$$

i.e. $\beta = 1/2$. This is a soft scenario, since we are still dealing with the translational symmetry [2].

However, a hard scenario for the spontaneous symmetry breaking can also take place. Indeed, if the translational (homogeneity) and rotational (isotropy) space symmetries are broken, and for some reason the soft scenario cannot be realized, the fluid motion has only one of the space fundamental symmetries remained - the Lagrangian relabeling symmetry [3]. In this case control on the distributed chaos is switched to the relabeling symmetry.

Due to the Noether's theorem conservation of helicity in inviscid fluids is a result of the relabeling symmetry

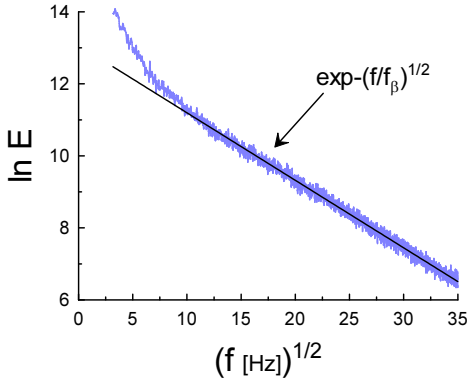

FIG. 1: Logarithm of the frequency power spectrum of the temperature fluctuations, measured at the wake centerline, against $f^{1/2}$.

[4],[5],[6],[7]. Therefore the helicity correlation integral (Levich-Tsinober invariant [8],[9],[10])

$$I = \int \langle h(\mathbf{x},t)\cdot h(\mathbf{x}+\mathbf{r},t)\rangle d\mathbf{r} \tag{5}$$

should be used in the scaling relation for the waves driving the distributed chaos, instead of the vorticity correlation integral (cf Eq. (1)),

$$v(\kappa) \propto\ I^{1/4}\ \kappa^{1/4} \tag{6}$$

i.e. $\alpha = 1/4$ in this case. Substituting this value of α in the Eq. (4) one obtains $\beta = 1/3$.

TURBULENT WAKE BEHIND CYLINDER

In paper Ref. [11] an experiment with a turbulent wake behind a slightly heated circular cylinder has been described. The experiment was performed in a wind

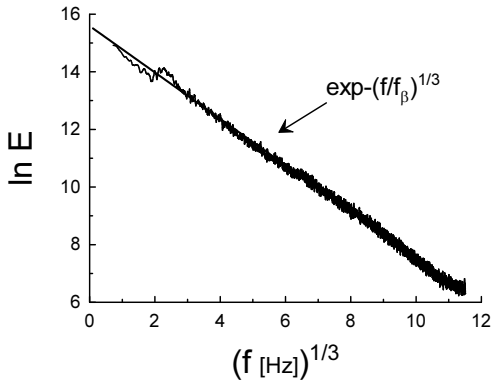

FIG. 2: Logarithm of the frequency power spectrum of the temperature fluctuations, measured away from the wake centerline, against $f^{1/3}$.

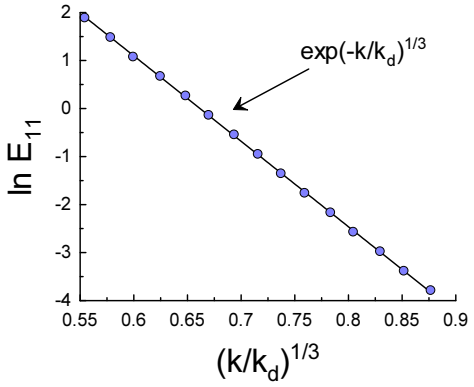

FIG. 3: Logarithm of normalised longitudinal energy spectrum against $(k/k_d)^{1/3}$ in the *non-classical* dissipation region of the distances from the grid (k_d is the Kolmogorov's scale). The only chaotic part of the spectrum is shown (corresponding to the insert in the Fig 5.4b of the Ref. [14]).

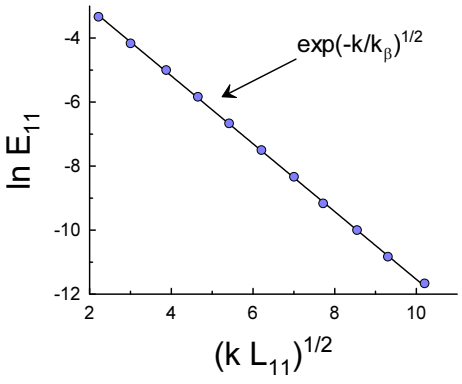

FIG. 4: Logarithm of normalised longitudinal energy spectrum against $(kL_{11})^{1/2}$ in the *classical* dissipation region of the distances from the grid. The only chaotic part of the spectrum is shown

tunnel with Reynolds number $Re_\lambda = 130$. The temperature fluctuations (as a passive scalar) were measured in this experiment with a cold-wire probe. Figure 1 shows power spectrum of the temperature fluctuations measured at the farthest downstream location (about 160 cylinder's radii) on the wake centerline. The scales in this figure are chosen to show (as a straight line) correspondence of the data to the spectrum Eq. (3) with $\beta = 1/2$ (the soft scenario). Figure 2 shows power spectrum of the temperature fluctuations measured away from the centerline (at distance of about three cylinder's radii). The scales in this figure are chosen to show correspondence of the data to the spectrum Eq. (3) with $\beta = 1/3$ (the hard scenario).

One can see that both the soft and hard scenarios are realized in the wake depending on conditions.

WAKES BEHIND GRIDS

Wakes behind grids are widely used in experiments in order to generate 'homogeneous' turbulence. Of course, the turbulence in the wakes of the grids is not homogeneous, especially near the grids (for small R_λ it is rather complex [12]). However, these wakes can be successfully used for studying the spontaneous translational symmetry breaking.

In series of recent papers Ref. [13] detailed experimental studies of the wakes behind different (active and passive) grids were reported. Here we will use the data obtained in these experiments and taken from Ref. [14]. We will be interested in the regular (passive) grids named in the Refs. [13],[14] as RG60 (a bi-planar intermediate-blockage square-mesh grid built from rectangular section bars) and RG230 (a mono-planar low-blockage grid similar to the RG60). The authors of the Refs. [13][14] used the Taylor estimate for the kinetic energy dissipation rate $\varepsilon \simeq C_\varepsilon u^3/L$, with u as the streamwise r.m.s. velocity and L as the longitudinal integral length-scale, in order to distinguish between the near and far wakes behind the grids. They called the (near) wake with non-constant C_ε as non-classical dissipation region. Outside this region C_ε is approximately independent on the Reynolds number in their experiments.

Figure 3 shows normalised longitudinal energy spectrum for two positions in the *non-classical* dissipation region of the distances from the grid (the data were taken from the insert in the Fig. 5.4b of the Ref. [14], the grid RG230, $R_\lambda = 300$ and 384). The scales in this figure are chosen to show (as the straight line) correspondence of the data to the spectrum Eq. (3) with $\beta = 1/3$ (the hard scenario). Figure 4 shows normalised longitudinal energy spectrum in the *classical* dissipation region of the distances from the grid (the data were

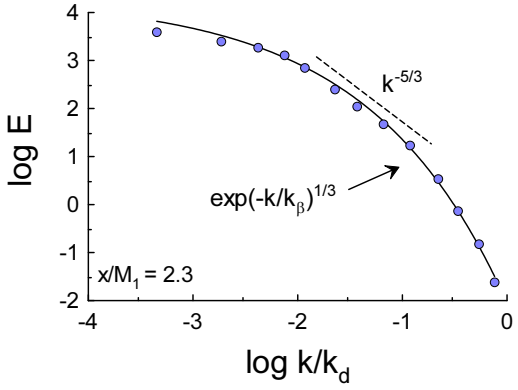

FIG. 5: Longitudinal energy spectrum near the multi-scale grid: $x/M_1 = 2.3$. The solid curve indicates the hard scenario.

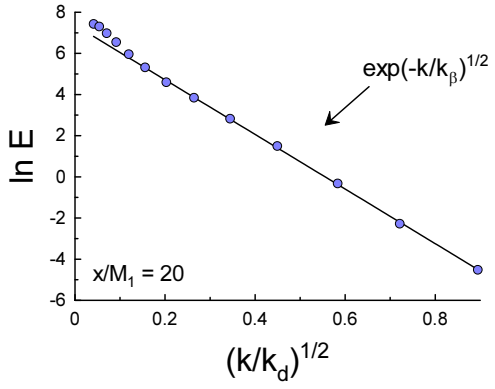

FIG. 7: The same as in Fig. 6 but in the scales chosen to show (as the straight line) correspondence of the data to the spectrum Eq. (3) with $\beta = 1/2$ (the soft scenario at large k/k_d).

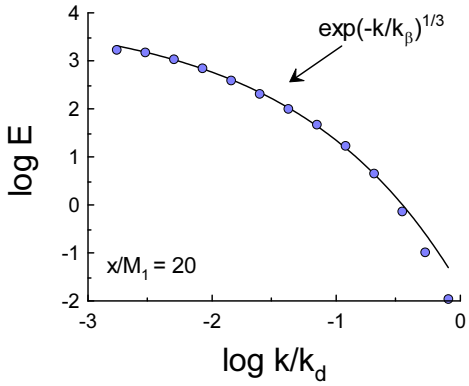

FIG. 6: Longitudinal energy spectrum at distance $x/M_1 = 20$ from the multi-scale grid. The solid curve indicates the hard scenario at small k/k_d.

taken from the Fig. 5.2b of the Ref. [14], the grid RG60, $R_\lambda = 120$). The scales in this figure are chosen to show (as the straight line) correspondence of the data to the spectrum Eq. (3) with $\beta = 1/2$ (the soft scenario).

In a recent paper Ref. [15] results of an experiment with multi-scale grids were reported. The large recirculating wind tunnel was used for this experiment (see for details Ref. [16]). The Reynolds number based on M_1 $Re_M = 6.0 \times 10^4$ (where M_1 is the largest mesh size for the multi-scale grid). The multi-scale grids inject energy in the flow at a large number of scales. In particular, at present experiment the geometric scales of the multi-scale grid are distributed about over the whole range of the turbulent flow spectrum.

Figure 5 shows (in the log-log scales) longitudinal energy spectrum near the multi-scale grid: $x/M_1 = 2.3$ (the data correspond to Fig. 9 of the Ref. [15]). The solid curve (the best fit) is drawn in order to indicate correspondence of the data to the spectrum Eq. (3) with $\beta = 1/3$ (the hard scenario). Unlike the above described situation (Fig. 3) the spectrum Eq. (3) with $\beta = 1/3$ covers about entire spectrum in this case. The dashed straight line with the slope -5/3 indicates a hint of the Kolmogorov scaling law.

Figure 6 shows analogous spectrum at distance $x/M_1 = 20$ from the grid (the data correspond to Fig. 8 of the Ref. [15]). It is interesting that at this distance the spectrum Eq. (3) with $\beta = 1/3$ covers a range corresponding to comparatively small values of k/k_d. Figure 7 shows the same data as in Fig. 6 but in the scales chosen to show (as the straight line) correspondence of the data to the spectrum Eq. (3) with $\beta = 1/2$ (the soft scenario). At the large k/k_d and x/M_1 turbulence is more homogeneous hence the soft scenario.

As in the previous section both the soft and hard scenarios are realized in the grid wakes depending on conditions.

WAKES BEHIND GRIDS IN SUPERFLUID

A liquid phase of ^{4}He is called He I with Navier-Stokes dynamics above $T_\lambda \simeq 2.17$ K, and He II (superfluid) below T_λ. The two-fluid model can be used for this superfluid composed of a Navier-Stokes component and a superfluid component with quantized vorticity and zero viscosity. The ratio $\rho_s/\rho = 0$ at T_λ and increases to 1 with $T \to 0$ K (ρ_s is density of the superfluid component and ρ is total density).

In a recent experiment reported in Ref. [17] a wake

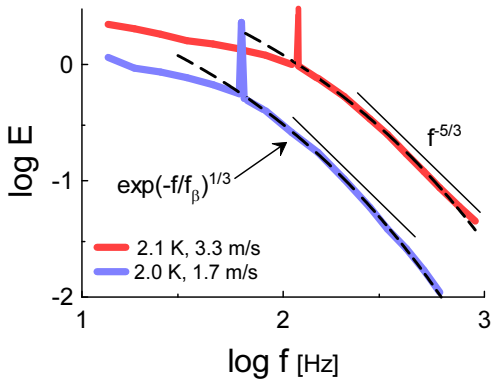

FIG. 8: Power spectra of velocity behind a grid in a superfluid (log-log scales, E is in arbitrary units).

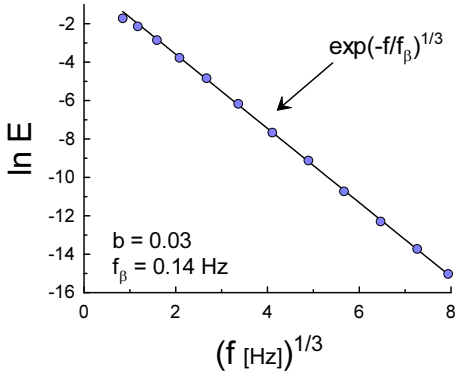

FIG. 9: Logarithm of normalised power spectrum of vertical component of the water velocity fluctuations for $b = 0.03$

behind a grid was studied above and below T_λ. In He I the grid mesh size Reynolds number $R_M \simeq 10^5 \sim 2\times10^6$, in He II $R_M \simeq 1.5 \times 10^4 \sim 2 \times 10^5$ (in the last case the quantum of circulation was used instead of viscosity in defining the Reynolds number).

Figure 8 shows velocity spectra obtained in this experiment at temperatures below T_λ at distance $x/M \simeq 138$ downstream the grid (the data were taken from Fig. 4 of the Ref. [17] and only relevant peaks are shown). The dashed lines (the best fit) indicate the stretched exponential spectrum Eq. (3) with $\beta = 1/3$ (the hard scenario) for the both observed spectra.

An interesting hint of a scaling (of Kolmogorov's type with $E \propto f^{-5/3}$) has been shown as a straight solid line for the upper spectrum (2.1 K, 3.3 m/s) in Fig. 8 (cf Fig. 5). This hint is discussed in detail in the Ref. [17] and has been also supported there by comparison with the Kolmogorov constant. Usually the range of the distributed chaos is not overlapped considerably with the scaling region because the exponential spectra are typical for smooth (sub)systems whereas the scaling spectra are typical for the rough ones. For $T < T_\lambda$ one could relate the overlapping to the two-fluid situation. But the problem with this explanation is that the spectral picture observed in this experiment for $T = 2.6$ K $> T_\lambda$ (3.3 m/s) is very similar to that presented in the Fig. 8.

TURBULENT BUBBLY FLOWS

The bubble wakes generate turbulence in surrounding liquid. It is known that even a tiny concentration of bubbles changes the velocity spectra cardinally [18]. It is typical for spontaneous symmetry breaking.

To quantify the phenomenon the 'bubblance' parameter was introduced in Ref. [19] (see also Refs. [18] and

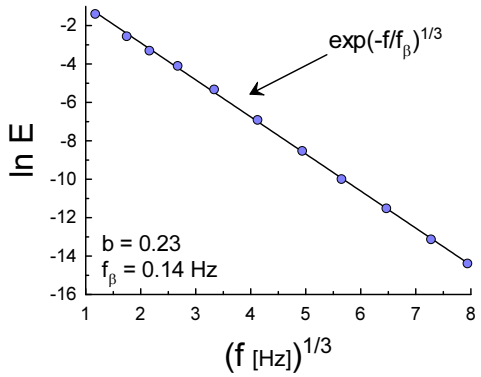

FIG. 10: The same as in Fig. 9 but for $b = 0.23$.

[20])

$$b = \frac{1}{2}\frac{\alpha U_r^2}{u_0^2} \tag{7}$$

with U_r as the bubble rise velocity in still liquid, u_0 as the typical velocity fluctuation in the liquid without of bubbles, and with α as concentration of the bubbles. This is a 'kinetic energy ratio' parameter and it can be relevant to the energy spectral analysis. The value $b = 0$ corresponds to single-phase situation (without bubbles). We naturally will be interested here in small values of the parameter b relevant to the spontaneous symmetry breaking.

In recent paper Ref. [18] the data obtained in an experiment with a wide range of the parameter b were presented (we will use these data obtained for small values of b). In this experiment an 8 m high vertical water tunnel, with an active grid generating coflowing turbulent upward bubbly flow, was used ($R_\lambda = 170$ for $b = 0$) .

Figure 9 and 10 show normalised power spectrum of vertical component of the water velocity fluctuations for $b = 0.03$ and 0.23 respectively (the data were taken

from Fig.6f of the Ref. [18]). The scales in these figures are chosen to show (as the straight line) correspondence of the data to the spectrum Eq. (3) with $\beta = 1/3$ (the hard scenario). It is worth noting that value of the parameter $f_\beta \simeq 0.14$ Hz is the same for these two cases (that can mean a tuning of the distributed chaos to this low-frequency value at the hard spontaneous symmetry breaking).

I thank K. R. Sreenivasan and P.-A. Krogstad for sharing their data, D. Lohse for attracting my attention to the experimental studies of his group and A. Pikovsky for explanations.

[1] A. C. Newell, B. Rumpf, V. E. Zakharov, Phys. Rev, Lett., **108**, 194502 (2012).
[2] A. Bershadskii, arXiv:1601.07364 (2016).
[3] J. E. Marsden et. al., arXiv:math/0005034 (2000).
[4] J.J. Moreau, Seminaire Danalyse Convexe, Montpellier 1977 , Expose no: 7 (1977)
[5] A. Yahalom, arXiv:solv-int/9407001 (1994); J. Math. Phys. **36** 1324 (1995).
[6] N. Padhye and P. J. Morrison, Phys. Lett. A **219**, 287 (1996).
[7] Y. Fukumotoa , H. Sakumab, Procedia IUTAM **7** 213 (2013) .
[8] E. Levich and A. Tsinober, Phys. Lett. A **93**, 293 (1983).
[9] A. Frenkel and E. Levich, Phys. Lett. A **98**, 25 (1983).
[10] E. Levich, Concepts of Physics **VI**, 239 (2009).
[11] P. Kailasnath, K.R. Sreenivasan and J.R. Saylor, Phys. Fluids A **5**, 3207 (1993).
[12] A. Bershadskii, Phys. Fluids **20**, 085103 (2008).
[13] P. C. Valente and J. C. Vassilicos, Phys. Fluids. **27**, 045103 (2015); J. Fluid Mech. **744**, 300 (2014); Phys. Rev. Lett. **108**, 214503 (2012); J. Fluid Mech., **87**, 300 (2011).
[14] Valente, arXiv:1307.6524 (2013).
[15] P.-A. Krogstad, http://www.tsfp-conference.org /proceedings/2013/v3/hom2a.pdf
[16] P.-A. Krogstad and P. A. Davidson, J. Fluid Mech. **680**, 417 (2011).
[17] J. Salort et al., Phys. Fluids **22**, 125102 (2010); arXiv:1202.0643 (2012).
[18] V. N. Prakash et al., J. Fluid Mech. **791**, 174 (2016).
[19] M. Lance and J. Bataille, J. Fluid Mech. **222**, 95 (1991).
[20] J. Rensen, S. Luther and D. Lohse, J. Fluid Mech. **538**, 153 (2005).